Science Applications, Inc.
Rolling Meadows, Ill.

Error Analysis of Penetrator Impacts On Bodies Without Atmospheres

by

Donald R. Davis

STAR Abstract

A preliminary analysis is performed of deployment schemes and resulting impacted errors of orbiter-launched penetrators at bodies without atmospheres. Penetrators are missile shaped objects designed to successfully implant subsurface experiments on planetary bodies at impact speeds of about 150 m/sec. Results are presented for lunar and Mercury penetrator missions. In both cases it is shown that the deployment mass and impact errors are minimized if the penetrators are dropped at low periapse orbit altitudes. Closed-loop guidance is required to monitor errors in the large penetrator retro braking maneuvers in order to subsequently align the penetrator for near-zero angle of attack impact.

Report No. SAI 1-120-194-T3

ERROR ANALYSIS OF PENETRATOR IMPACTS ON BODIES WITHOUT ATMOSPHERES

by

Donald R. Davis

Science Applications, Inc.
5005 Newport Drive, Suite 305
Rolling Meadows, Illinois 60008

for

Planetary Programs Division
Office of Space Science
NASA Headquarters
Washington, D. C.

Contract No. NASW-2613

February 1975

FOREWORD

This study was performed between November 1974 and February 1975 as part of the task schedule completed by Science Applications, Inc. for the Planetary Programs Division of OSS/NASA under Contract No. NASW-2613. The results are intended to assist NASA in advanced planning of planetary surface missions. Specifically, the objective of the report is to provide a preliminary evaluation of the feasibility of penetrator deployment at targets without atmospheres. If identified control problems are not unreasonably complex, further detailed analysis can be supported to bring the gasless planet penetrator design to a level of design definition compatible with planning requirements.

The author expresses his appreciation to E. Reese of Sandia Laboratories, to F. Jordan and C. Kohlhase of JPL for valuable technical inputs, and to A. Friedlander and J. Niehoff of SAI for many stimulating conversations and suggestions.

SUMMARY

Penetrators are missile shaped objects designed to implant electronic instrumentation in a wide variety of surface materials with a nominal impact speed around 150 m/sec. They have been used successfully in many terrestrial applications over the past decade. Recently they have also been proposed for post-Viking/75 Mars exploration.[1,2,3] The most significant advantage of planetary penetrators is that they avoid the high cost of soft landers without imposing the extreme impact conditions of hard surface landers on the payload. An initial favorable response by the science community to the exploration potential of Mars penetrators has prompted an interest in the application of this concept to in situ subsurface studies of other terrestrial bodies and planetary satellites. Unlike Mars many of these objects do not have atmospheres. A first order feasibility question has thus arisen: "Can penetrators be successfully guided to the required near-zero angle-of-attack impact conditions in the absence of an atmosphere?" A preliminary answer to this question is the purpose of this report.

The scope of the analysis includes two potential targets, i.e. the moon and Mercury, involves several different penetrator deployment modes, and focuses on impact errors arising from open-loop and closed-loop deployment control systems. Successful penetrator implacement requires: 1) that the impact speed be controlled, nominally to 150 m/sec; 2) that the penetrator angle of attack, measured between the longitudinal axis and velocity vector, be in the range 0^{o} - 11^{o} at impact; and 3) that the impact flight path angle be within 15^{o} of vertical. It is the errors in these terminal conditions that are the principal concern of this study.

The best mode of penetrator deployment identified uses an orbiting spacecraft as a penetrator launch platform. This mode, labeled the Intermediate Ellipse Transfer (IET) Mode, is depicted in Table S1. Prior to deployment the orbiter is first placed in an elliptical low-periapse altitude orbit. The penetrator is launched at periapse with a retro motor which kills its orbital velocity. It is then pitched over and allowed to free-fall to the surface. The deployment characteristics of the IET Mode are also summarized in Table S1. The initial orbit is circular at the moon and elliptical at Mercury. A free-fall impact velocity of 150 m/sec means that the periapse altitudes of these orbits must be lowered to 7 km and 3 km at the moon and Mercury, respectively, prior to penetrator deployment. This should not be a problem at the moon, but at Mercury a combination of several orbital maneuvers, onboard radar altimetry, and solar perturbation control will be necessary to achieve the very low altitude of 3 km. Also it will be undesirable to leave the orbiter in this orbit for more than several revolutions due to the impact hazard without continuous control. The penetrator retro ΔV requirements to kill the orbital periapse velocity are a nominal 1700 m/sec at the moon, but over 4 km/sec at Mercury. Assuming a penetrator impact mass of 31 kg (i.e. the Mars design), 10 kg for the attitude control system, and a single stage solid motor retro system, the total deployed mass of each penetrator is 81 kg at the moon and 251 kg at Mercury. These values can be compared with a deployed mass of only 50 kg at Mars where atmospheric braking is used to slow the penetrators.

Key results of the deployment error analysis are summarized in Table S2. The errors in DSN tracking of the orbiter's state at deployment are small and have little effect on any of the impact conditions except impact location. The primary error source for impact velocity and angle-of-attack errors is penetrator retro execution errors. The execution

Table S1

REFERENCE DEPLOYMENT MODE

- INTERMEDIATE ELLIPSE TRANSFER (IET) DEPLOYMENT SCHEMATIC

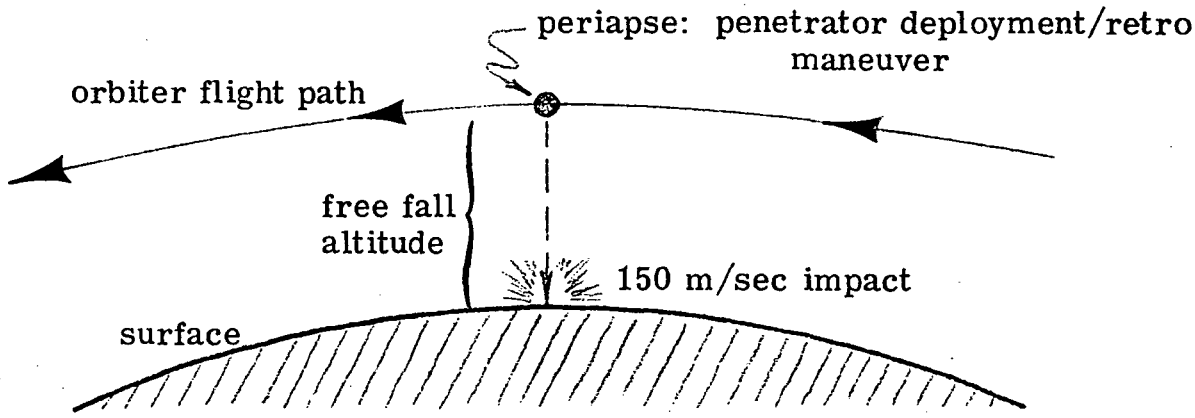

- IET DEPLOYMENT CHARACTERISTICS

	Moon	Mercury
Initial orbit periapse altitude (km)	100	600
Initial orbit eccentricity	0.0	0.8
Penetrator deployment periapse altitude (km)	7.0	3.0
Penetrator retro impulse (m/sec)	1698	4065
Penetrator impact velocity (m/sec)	150	150
Penetrator impact mass (kg)	31	31
Penetrator deployment mass[a] (kg)	81	252

a. Just prior to single stage solid retro.

Table S2

PENETRATOR DEPLOYMENT ERROR SUMMARY[a]

	Moon	Mercury
• DSN TRACKING ERRORS AT DEPLOYMENT		
Altitude (m)	100	150
Velocity (m/sec)	10	24
• RETRO EXECUTION ERRORS (m/sec)		
Radial ($\dot{x}$)	30	71
In Path ($\dot{y}$)	26	61
Cross Path ($\dot{z}$)	30	71
• OPEN LOOP IMPACT ERRORS		
Speed (m/sec)	8	41
Angle of Attack (deg)	15	36
Miss Distance (km)	15	21
• CLOSED-LOOP IMPACT ERRORS		
Speed (m/sec)	8	41
Angle of Attack (deg)	2	2
Miss Distance (km)	15	21

a. 3σ errors of IET deployment mode

errors shown in the table are scaled to the magnitude of the impulse assuming 3σ pointing errors of 1.0^{o} and 3σ magnitude errors of 1.5%. The affect of these errors on impact conditions are shown as open-loop impact errors. The critical errors are in impact angles of attack which are dominated by errors in the terminal flight path angle. With a maximum acceptable impact angle of attack of 11^{o} required to successfully penetrate even very soft soils, it is readily seen that the open-loop control mode is unsatisfactory having 3σ values of 15 degrees at the moon and 36 degrees at Mercury. Adding an accelerometer triad to the penetrator to monitor the retro burn errors easily reduces the angle of attack errors to very small values (2^{o}) as can be seen by the tabulated closed-loop error summary. It should be noted, however, that nothing is done in the closed-loop mode to correct the execution errors, the attitude control system just accomodates them. Hence, the impact flight path angle, at Mercury in particular, may still be larger than the 15^{o} off-vertical limit desired by some of the penetrator experiments, e.g. seismometers.

As an overall conclusion to this analysis, the deployment of lunar penetrators appears to pose no unreasonable performance or control requirements. Conversely, the low deployment altitudes, the large retro mass, and large retro execution errors all raise feasibility questions for a Mercury penetrator mission. More detailed analysis will be required to resolve these issues and is recommended.

TABLE OF CONTENTS

1. INTRODUCTION

The use of subsurface penetrators in a variety of terrestrial scientific applications has been carried out over the past decade.[1] These applications have included polar ice depth measurements and ocean floor sediment studies, along with more conventional impact studies into a variety of surface materials. Recent studies have considered the application of penetrators to the subsurface exploration of Mars as part of a post-Viking/75 Mars scientific mission.[1, 2, 3]

The rationale for such missions is presented in references 1 and 2. Penetrators could return data on upper crustal heat flow, seismic measurements, physical properties measurements, geochemistry, and other in situ surface characteristics depending on the specific application. Successful penetrator deployment requires penetration to at least a one-meter depth in the hardest materials with maximum peak decelerations held to less than 2000 earth g's for payload integrity. Penetrators were designed to meet these constraints for a wide variety of surface material. The Mars penetrator has a detachable afterbody which contains an antenna that remains on the surface and serves as a relay link between the buried forebody and the orbiting parent spacecraft. The forebody penetrates to a depth between 1 and 15 meters, depending on the surface materials. Table 1 gives a brief summary of the Mars penetrator as described in reference 1. To achieve the desired penetration depths requires an impact speed of about 150 m/s.[1] The impact flight path angle should be greater than 75^{o} to insure proper seismic measurements with fixed body detectors. Finally, the impact angle of attack (the angle between the longitudinal axis of the penetrator and the velocity vector at impact) is constrained to a small value. As the penetrator very quickly aligns itself with the velocity vector after impact, misalignment will give rise to large shear forces which could lead to penetrator failure. The

Table 1

MARS PENETRATOR CHARACTERISTICS

• MASS SUMMARY	
at orbiter deployment	50 kg
at impact	31 kg
science/electronics budget	7 kg
• LENGTH	140 cm
• PRINCIPAL DIAMETER	9 cm
• IMPACT CONSTRAINTS	
speed	140-170 m/s
direction	vertical $\pm 15^{o}$
angle of attack (rock)	$<3^{o}$
(loess)	$<11^{o}$
• PEAK DECELERATIONS	
forebody (science)	<1800 g for 5 ms
afterbody (transmitter)	<18000 g for 3 ms
• DEPTH OF PENETRATION	1-15 m

magnitude of the allowable misalignment depends significantly on the impacted material. For rather unconsolidated surfaces such as loess, the alignment error could be as much as 11^{o}, whereas for rocky surfaces 3^{o} would be a more reasonable upper bound. These penetrator impact constraints are also summarized in Table 1.

For the Mars studies, the penetrator may be deployed from either a Pioneer or Mariner class spacecraft in orbit about Mars. The penetrator and its aeroshell are inserted on an entry trajectory into the Martian atmosphere using a small solid rocket motor. Attitude control and orientation is provided by the parent spacecraft for this maneuver. Atmospheric deceleration and entry heating are controlled by the aeroshell design and the atmospheric entry angle. After the descent velocity becomes subsonic a secondary deceleration system, e.g. a parachute, is deployed for final terminal velocity and attitude control.

The penetrator science return is probably higher for a body such as Mercury than it is at Mars, because no prior in situ subsurface measurements are likely to have been made. Initial seismic and heat flow measurement would greatly increase our knowledge of Mercury's interior and its massive heavy core. For lunar applications, although additional measurements might not be as significant as the initial Apollo and Surveyor data, they would allow sampling of different lunar geologic features and permit a comparison of heat flow in the lunar uplands with the Apollo mare measurements. Seismic measurements could supplement or extend those currently being returned from the ALSEP stations. Hence, there exists a general interest in the broader application of the penetrator concept to solar system exploration.

The objective of this study is to examine the errors associated with penetrator deployment at bodies without atmospheres, with Mercury and the moon being emphasized in the analysis. For such bodies, the impact speed, flight path angle and attitude must be controlled through propulsive maneuvers and systems associated with the penetrator. Initially the penetrator deployment system is assumed to be "open loop", i.e. no onboard measurements are taken and errors in impact conditions are calculated by propagating the errors resulting from, a) the orbit determination process, b) maneuver execution, and c) attitude control system pointing, down to impact. It will be shown that an "open-loop" deployment scheme cannot meet the impact constraint requirements presented in Table 1. Consequently, a "closed-loop" approach is also investigated using several different types of onboard measurements. This study is not intended to be a mission analysis report, but rather to ascertain the magnitude of the problem for penetrator deployment onto gasless bodies. Hence, the impact of orbital operations necessary or desirable for penetrator deployment on other mission objectives has not yet been examined. Subsequent sections of this report describe the penetrator deployment modes, error sources and error analysis, and the types of onboard measurements necessary to reduce terminal errors.

2. PENETRATOR DEPLOYMENT MODES

The penetrator impact constraints (see Table 1) require a near vertical approach to the surface with a planned terminal velocity of 150 m/sec. These conditions imply a rectilinear free-fall descent from some altitude at which the penetrator is brought to rest. This rest altitude will depend on both the impact body mass and the desired impact speed. Rest altitudes and free-fall times are given in Table 2 for two impact speeds, 150 m/sec and 300 m/sec. The lower value of 150 m/sec is the Mars penetrator design point and is considered a good compromise between impact deceleration and penetration for a wide range of impact materials. The higher value of 300 m/sec is probably an upper bound on impact speed. For most rocky surfaces (with soil constants[1] less than 1.5) peak decelerations would exceed 2000 g's in the forebody at this speed, and for loose soils such as loess (with soil constants greater than 10) the depth of penetration would exceed 20 m. These values assume the same goemetric design as the Mars penetrator.

The finite intrinsic rotational speed of the impact body surface will add a normal component of velocity to the free-fall impact speed with the result being only a nearly rectilinear rather than truly rectilinear terminal descent. For the two bodies of primary interest in this analysis, the moon and Mercury, their maximum surface rotational speeds are 4.6 and 3.0 m/sec, respectively, and occur, of course, along the equator. Using a minimum vertical impact speed of 150 m/sec, the maximum off-vertical impact angles are 1.75^{o} and 1.15^{o}, respectively. As these angles are small and would be even smaller for non-equatorial impact sites and higher impact velocities, the analysis and terminology of a true rectilinear descent is used in this report.

Table 2

PENETRATOR FREE FALL CHARACTERISTICS AT ATMOSPHERELESS BODIES

Object	Mass (10^{24}g)	Surface Radius (km)	Surface Gravity (m/sec^2)	Impact Speed (m/sec)	Rest Altitude (km)	Fall Time (sec)
Mercury	330.2	2439	3.70	150	3.0	41
				300	12.2	82
Moon	73.5	1738	1.62	150	7.0	93
				300	28.2	189
Ceres	1.2	478	0.35	150	34.0	467
				300	176.0	1308
Io	91.0	1820	1.83	150	6.2	82
				300	24.9	167
Europa	48.7	1550	1.35	150	8.4	112
				300	34.0	228
Ganymede	149.0	2635	1.43	150	7.9	105
				300	31.8	213
Callisto	106.4	2500	1.14	150	9.9	133
				300	40.3	270

It is assumed that a parent spacecraft carries the penetrators into an initial orbit about the target body from which it can selectively deploy the penetrators and frequently communicate with them after they are implanted. Once in orbit a penetrator can be placed on a rectilinear descent ellipse (for a normal surface impact) at any time by killing its orbital velocity. The two extreme points of deployment considered in the analysis are at the orbit periapsis and apoapsis. The two modes associated with these orbit extremes are illustrated in Figure 1. The Intermediate Ellipse Transfer (IET) Mode first puts the spacecraft on a Hohmann transfer ellipse with a periapsis altitude equal to the desired rest altitude (see Table 2). The penetrator is deployed at periapsis with a ΔV which kills its orbital velocity and free falls to the surface. The second of the two modes, the Rectilinear Ellipse Transfer (RET) Mode, stops the penetrator at apoapsis from which it starts its free fall. As it nears the surface a second ΔV again stops the penetrator from which point (i.e. the rest altitude) it accelerates to impact at the desired speed.

Deployment of penetrators from orbit with minimum impulse expenditure requires a low altitude near-circular orbit for either mode presented in Figure 1. Such an orbit is easily attained at the Moon, but at Mercury elliptical orbits are preferred due to the limited capacity of current propulsion systems to deliver useful payload into Mercury orbit. Reference initial spacecraft orbits for this analysis were selected with these considerations in mind; they are summarized at the beginning of Table 3. For lunar missions the initial orbit is circular with a low altitude of 100 km. For Mercury missions a 0.8 eccentricity orbit with an initial periapse altitude of 600 km was chosen from reference 4.

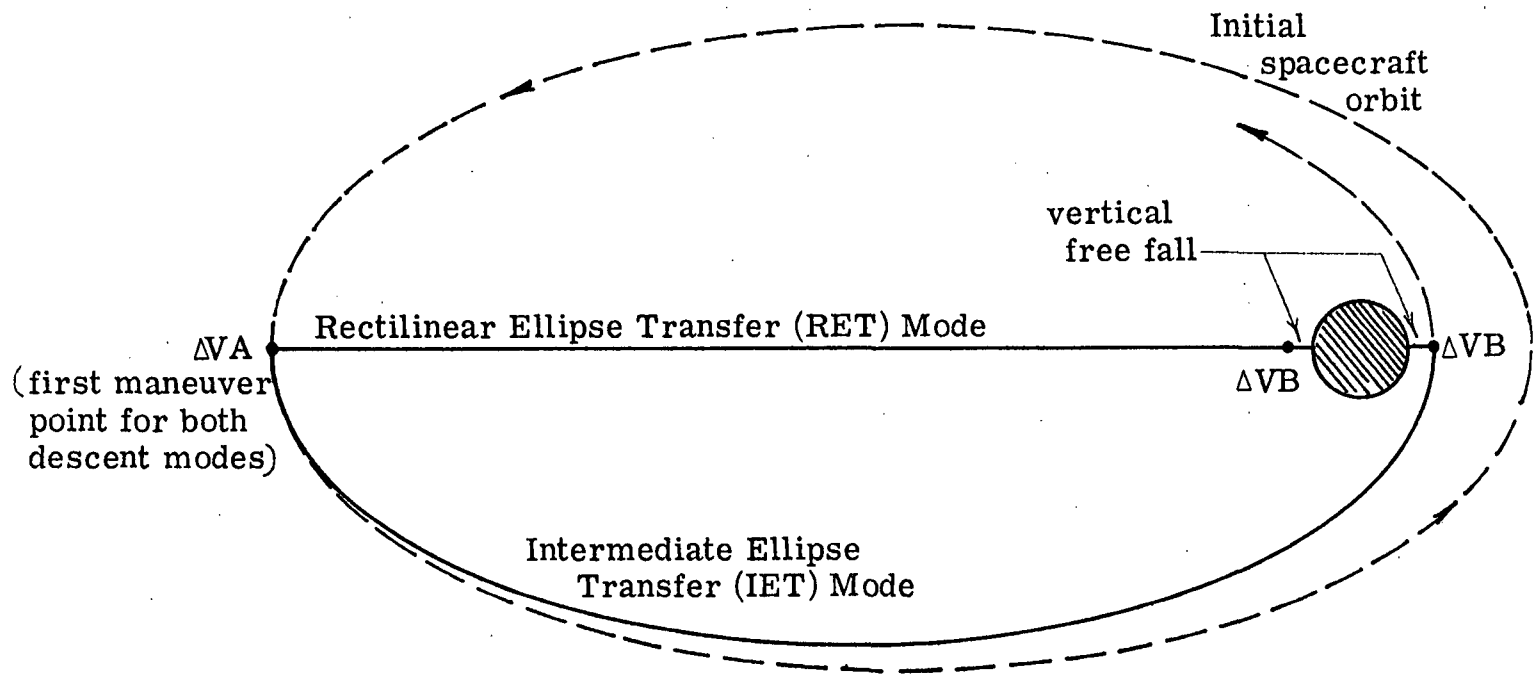

FIG. 1. PENETRATOR DEPLOYMENT MODES

The deployment impulse requirements at both the moon and Mercury are also summarized in Table 3 for both deployment modes presented in Figure 1, using both 150 and 300 m/sec impact speeds. From the data in the table it is readily seen that the IET Mode results in lower impulse requirements; the difference in impulse requirements between the two impact speeds is negligible. Also, the requirements at Mercury, due to the higher energy spacecraft orbit, are more than twice as large as the lunar cases. Variations from the nominal IET and RET Mode deployment schemes were briefly investigated with no significant difference found in the total impulse requirements. Included in the variations were 1) performing ΔVA in the RET Mode 10^{o} off apoapse, 2) employing a 10^{o} off-normal terminal descent, and 3) reducing the initial Mercury apoapse altitude to 9700 km. The largest reduction in the deployment impulse, due to reducing the Mercury apoapse altitude, was less than 4% of the total requirement.

Although the IET Mode readily produces the lowest impulse requirement it also creates the greatest risk to mission success since the spacecraft must come very close to the surface before releasing the penetrator, only 3 km at Mercury if an impact speed of 150 m/sec is required. In fact, drawing on results presented below in Section 4, the 3σ periapse altitude dispersions resulting from the ΔVA maneuver are about 8.4 km. Consequently, there exists an unacceptable chance that the spacecraft would crash if it attempted to reduce the periapse altitude as required in one apoapse maneuver. This can be remedied by reducing the periapse altitude in steps, separated by periods of orbit tracking and radar altimeter measurements in the vicinity of periapse. Alternatively, at Mercury, solar perturbations might be used to advantage producing the same desired reduction in periapse altitude.

Table 3

IMPULSIVE PENETRATOR DEPLOYMENT REQUIREMENTS

	Moon	Mercury
• INITIAL SPACECRAFT ORBITS		
Periapse Altitude (km)	100	600
Apoapse Altitude (km)	100	24880
Eccentricity	circular	0.8
Period (hours)	2.0	22
• DEPLOYMENT IMPULSE REQUIREMENTS (m/sec)		
o IET Mode - 150 m/sec impact		
ΔVA[a] (see Fig. 1)	21	38
ΔVB	1698	4065
Total Impulse	1719	4103
o IET Mode - 300 m/sec Impact		
ΔVA[a]	16	37
ΔVB	1683	4057
Total Impulse	1699	4094
o RET Mode - 150 m/sec Impact		
ΔVA	1632	399
ΔVB	536	4049
Total Impulse	2168	4448
o RET Mode - 300 m/sec Impact		
ΔVA	1632	399
ΔVB	471	4041
Total Impulse	2103	4440

a. ΔVA maneuver is made by the spacecraft propulsion system for the IET Mode.

The magnitude and direction of periapse altitude changes resulting from solar perturbations depend upon the orbit geometry and orientation. To successfully reduce the periapse altitude to a very small value without impacting the surface requires that the orbit to orbit change become vanishingly small as the final value of periapse is approached. A numerical analysis of various Mercury orbit conditions was performed for mission launch opportunities in 1980, 1985, and 1988 to see if orbits with this characteristic exist. Results from the analysis are presented in Figures 2 and 3. From these figures it can be seen that the aim angle (measured clockwise in the impact plane from the $\overline{T}$ axis to the aim vector, $\overline{B}$) controls the direction of periapse change. Using these results, the periapse histories for two specific orbits are tabulated in Table 4 which have the desirable attributes of near zero change near the planet's surface. The data illustrate that orbits can be found which permit the consideration of very close approaches to Mercury's surface.

In all the above discussion the principal concern has been the very low altitude requirement at Mercury required by the IET Mode in order to satisfy a 150 m/sec impact constraint. It should be noted from Table 2 that doubling the impact speed to 300 m/sec would raise the periapse altitude of the intermediate transfer ellipse from 3 km to a more comfortable 12 km, but would restrict the range of soils the penetrator could successfully impact. The evaluation of such a trade-off was not considered as part of this study. Suffice it to say that using solar perturbations as part of the periapse reduction strategy might reduce the impact hazard, but does add a new constraint on orbit orientation (particularly inclination and location of periapse) which will complicate the orbit selection process for the mission designer.

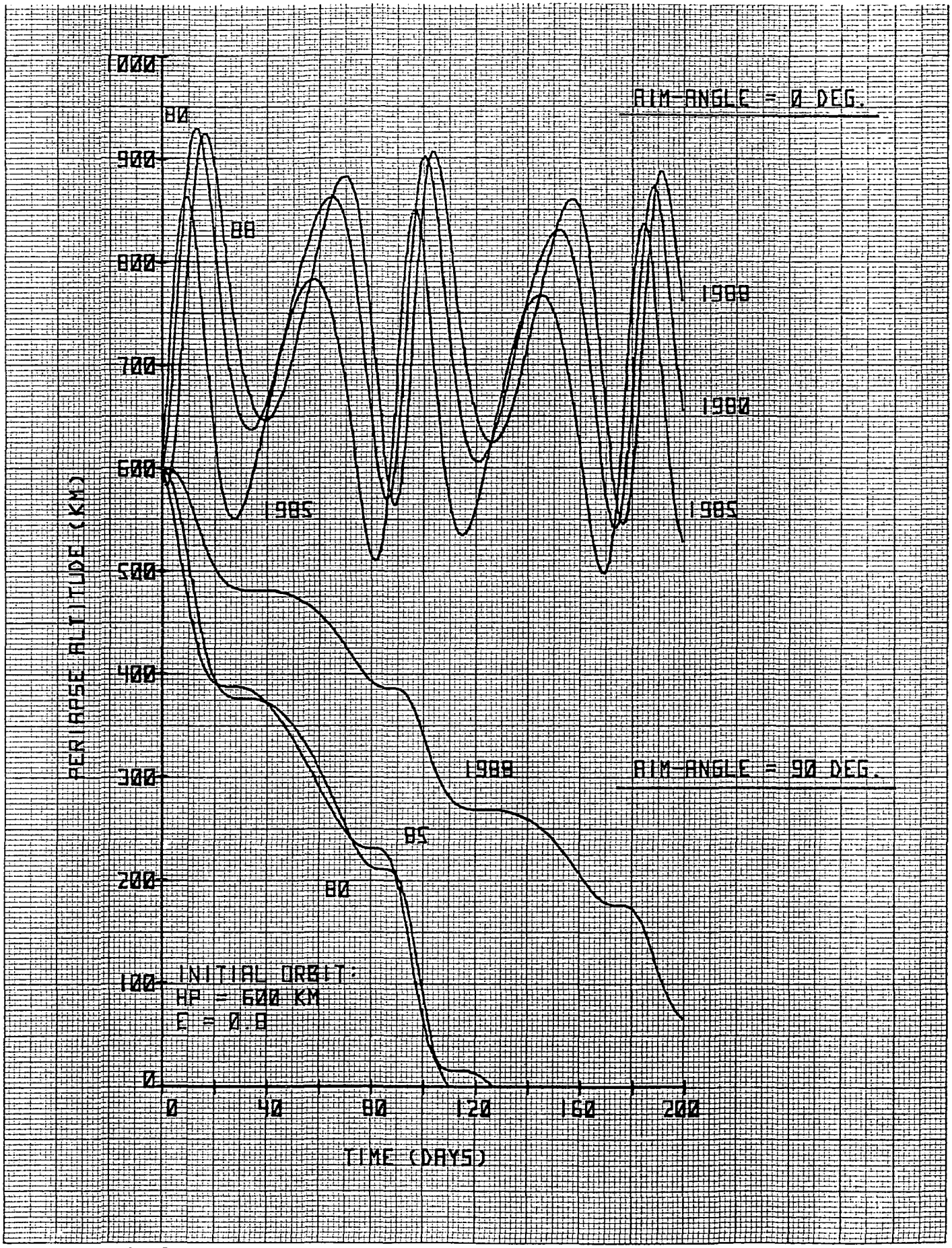

FIG. 2. AIM ANGLE EFFECT ON MERCURY ORBIT SOLAR PERTURBATIONS FOR THREE MISSION OPPORTUNITIES

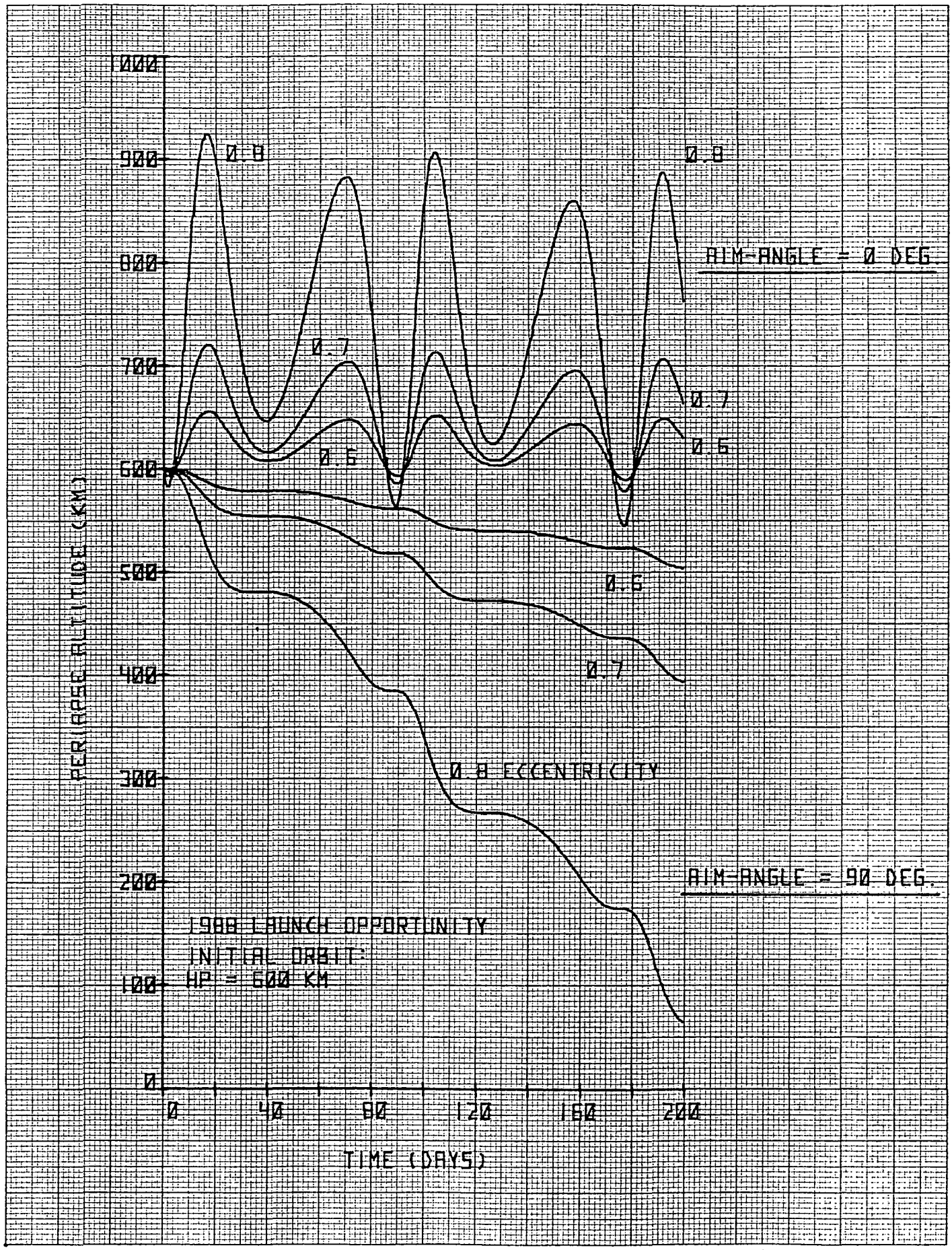

FIG. 3. AIM ANGLE EFFECT ON MERCURY ORBIT SOLAR PERTURBATIONS FOR THREE ORBIT ECCENTRICITIES

Table 4

SOLAR PERTURBED PERIAPSE HISTORIES OF MERCURY ORBITS

	Launch Opportunities	
	1980	1988
• ORBIT PARAMETERS		
Period (hrs)	22	22
Eccentricity	0.8	0.8
Initial Periapse Altitude (km)[a]	138	59
Initial Epoch	14 Apr 82	17 Sep 90
• PERIAPSE ALTITUDE HISTORIES (km)		
Orbit No. 0	138.0	59.0
5	132.6	58.7
10	115.0	55.7
15	85.4	47.8
20	53.5	36.3
25	28.2	24.5
30	12.9	15.1
35	5.9	8.9
40	3.8	5.6
42	3.6	4.8
44	3.5	4.3
46	3.5	4.0
48	3.5	3.8
50	3.3	3.7
52	3.0	3.7
54	2.4	3.7

a. Initial periapse altitude is reduced from the baseline altitude of 600 km by a spacecraft apoapse maneuver.

A preliminary estimate of the weight of the entire penetrator deployment system can be obtained by using the impact mass of the Mars penetrator design, i.e. 31 kg as presented in Table 1. To this should be added a 10 kg allowance for attitude control, sensors and control logic for guiding the penetrator between deployment and impact. For the IET Mode a minimum of only one retro motor is needed to kill the intermediate ellipse periapsis velocity. For the Mercury mission, however, a two-staged retro system will more effectively kill the large periapsis velocity. For the RET Mode at least two retro motors are needed if a simple solid propellant system is used. The first motor kills the orbital speed at apoapse and the second motor brakes the fall of the penetrator just prior to impact. A third motor might be used in the case of Mercury to split the large braking maneuver required. A summary of penetrator predeployment masses at the moon and Mercury is given in Table 5 for both deployment modes using the various staging strategies just discussed. A solid propellant specific impulse of 290 sec and a useful stage mass fraction of 90% has been assumed in generating the results which are for 150 m/sec impacts. Compared with the 50 kg predeployment mass of the Mars penetrator, these data reflect much higher requirements - from almost two to nearly six times as much mass. Additional staging at Mercury does reduce the mass requirements by about 14%, but also complicates the maneuver sequence. On the basis of mass considerations alone, the IET Mode for lunar penetrators still appears tractable. At Mercury, however, considering the difficulty with placing mass into orbit with current propulsion systems, the large retro mass requirements may pose a significant limitation on the penetrator mission concept.

Table 5

PENETRATOR PREDEPLOYMENT MASS (KG) SUMMARY

	Moon		Mercury		
	1-Stage	2-Stage	1-Stage	2-Stage	3-Stage
• IET MODE[a]					
Penetrator Impact Mass[b]	31	-	31	31	-
Control System Mass	10	-	10	10	-
Retro System Mass[c]	40	-	210	175	-
Total Predeployment Mass	81	-	251	216	-
• RET MODE					
Penetrator Impact Mass[b]	-	31	-	31	31
Control System Mass	-	10	-	10	10
Retro System Mass[c]	-	58	-	256	215
Total Predeployment Mass	-	99	-	297	256

a. Assume spacecraft is responsible for ΔVA (see Figure 1)

b. Based on Mars penetrator design; impact speed = 150 m/sec

c. Assumes solid retro system; Isp = 290 sec; stage mass fraction = 0.9 and for multistage systems, 2% of the stage weight above the retro is allowed for interstage connection.

3. ERROR SOURCES FOR PENETRATOR DEPLOYMENT

As successful penetrator implantation must be achieved through impulsive maneuvers and active penetrator attitude control, it is imperative to understand how well terminal constraints can be met using active systems. Errors in the final conditions arise primarily from two sources: 1) uncertainty in our measurement of the basic variables, i.e. spacecraft state vector, planetary topography, etc. and 2) errors introduced by spacecraft systems, i.e. maneuver execution errors and attitude control errors.

The orbit determination (O. D.) error model used in this study was obtained from JPL, and represents the O.D. errors in DSN tracking of planetary orbiters after several initial orbits have been tracked and utilized to improve a priori estimates of gravitational parameters. Figure 4 defines the geometry used in this formulation. The x-y plane is in the plane of the orbit and z is parallel to the orbital angular momentum vector. The 3σ uncertainties in the state vector are taken to be:

$$\Delta y = .006r,$$
$$\Delta z = .006r,$$
$$\Delta \dot{x} \simeq 10^{-2} \Delta y,$$
$$\Delta \dot{x} = .006\ v \cos \gamma,$$
$$\Delta \dot{y} = .006\ v \sin \gamma,$$
$$\Delta \dot{z} = .006\ v \sin \gamma.$$

In these equations, r is the magnitude of the radius vector to the spacecraft, v is the orbital speed of the spacecraft and γ is its flight path angle. The errors are assumed to be uncorrelated. Note that at apoapse and periapse, where the flight path angle is zero, the uncertainty in the tangential component of velocity is very small, with essentially all of the uncertainty being in the radial component. This arises not from

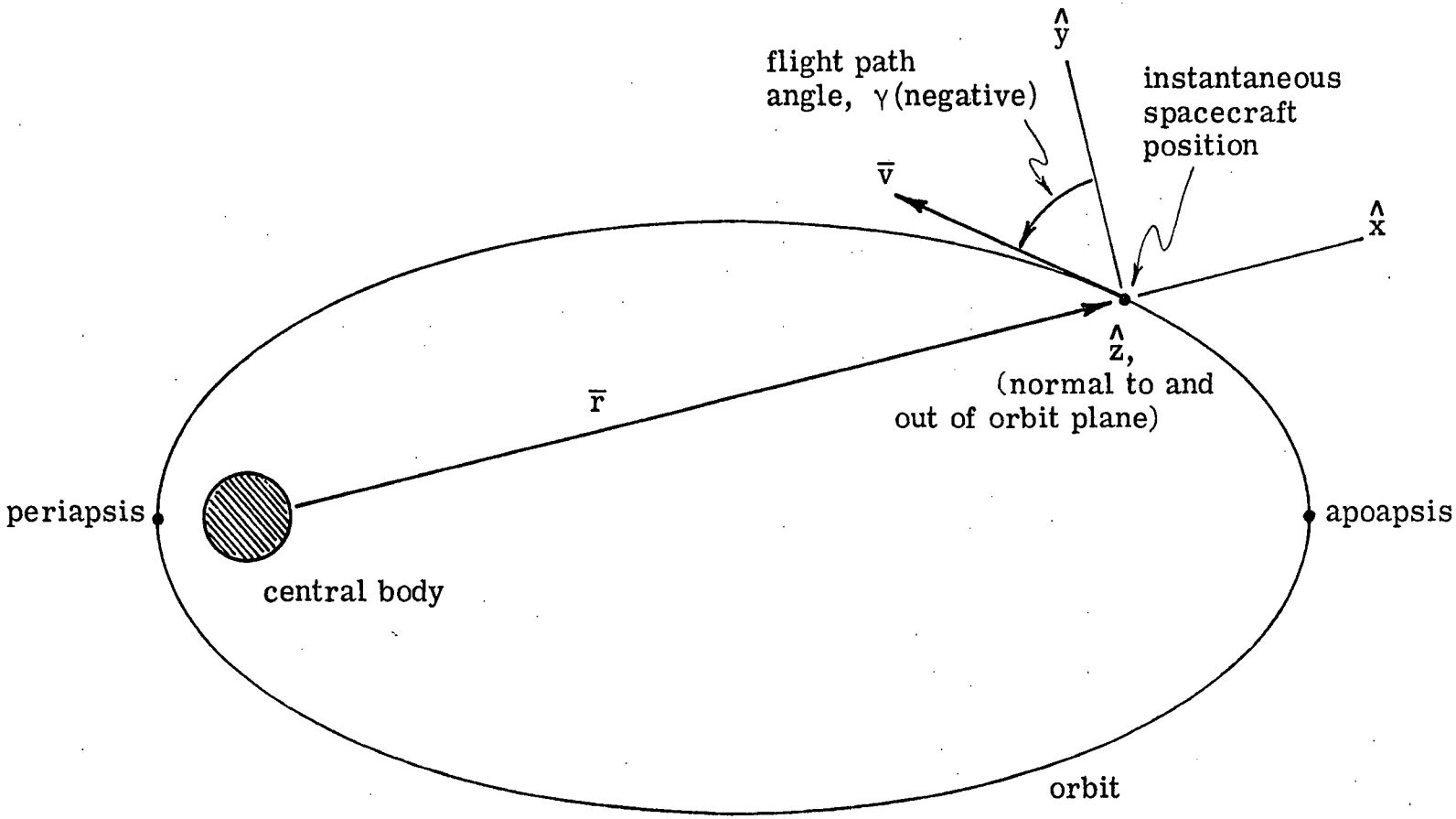

FIG. 4. COORDINATE SYSTEM ($\hat{x}$, $\hat{y}$, $\hat{z}$) FOR ERROR FORMULATION

uncertainty in the timing at which the spacecraft is at apsis, but rather from the uncertainty in the radius of the apsis location itself. The same formulation for O.D. errors is also used for circular orbits, i.e. for the lunar missions, and should be conservative for this case. Table 6 summarizes the resulting O.D. uncertainties for the nominal orbits used in this study.

The maneuver execution errors were formulated in terms of the variation in the magnitude and direction of the ΔV vector from nominal conditions, representing shut-off timing errors and the errors in the attitude control system in orientating and holding the spacecraft during the burns. The nominal 3σ impulse error was taken to be 1.5% of ΔV magnitude and orientation errors of 1.0^{o} were adopted for both inplane and out-of-plane pointing. Table 7 gives the resulting velocity errors with both descent modes beginning from the nominal Mercury and lunar orbits, and assuming an impact speed of 150 m/sec.

In a real application, the pointing errors will be related to the type of attitude control system used. A spin stabilized system is not well suited for penetrators since they are not dynamically stable when rotating about their roll axis. Furthermore, it would be difficult to pitch a spinning penetrator through 90^{o}, particularly after the periapse impulse (ΔVB) of the IET Mode. Hence, three axis stabilization appears preferable for penetrators based on initial consideration of the deployment requirements at atmosphereless bodies.

Table 6

ORBIT DETERMINATION UNCERTAINTIES[a]

	Lunar Circular Orbit (100 km alt)	Mercury e = 0.8 Orbit	
		Periapse (600 km alt)	Apoapse (24880 km alt)
Δx (km)	0.1	0.2	1.6
Δy (km)	11.0	14.5	164
Δz (km)	11.0	14.5	164
$\Delta \dot{x}$ (m/sec)	9.8	24.4	2.4
$\Delta \dot{y}$ (m/sec)	~0	~0	~0
$\Delta \dot{z}$ (m/sec)	~0	~0	~0

a. 3σ values

Table 7

MANEUVER EXECUTION ERROR SUMMARY[a]

	Lunar Cases				Mercury Cases			
	IET Mode		RET Mode		IET Mode		RET Mode	
	ΔVA	ΔVB	ΔVA	ΔVB	ΔVA	ΔVB	ΔVA	ΔVB
$\Delta \dot{x}$ (m/sec)	.4	29.6	28.5	8.0	.7	70.9	7.0	61.0
$\Delta \dot{y}$ (m/sec)	.3	25.5	24.5	9.3	.6	61.0	6.0	71.0
$\Delta \dot{z}$ (m/sec)	.4	29.6	28.5	9.3	.7	70.9	7.0	71.0

a. 150 m/sec impact speed

4. OPEN-LOOP ERROR ANALYSIS

The parameters of interest (dependent variables) for penetrator deployment are speed, flight path angle at impact, and miss distance, defined as the surface range between the nominal impact point and the perturbed impact point. Also, errors in the altitude of the ΔVB point (see Fig. 1, pg. 8) for both the IET and RET Modes are of concern. For each variable of interest, q, a sensitivity matrix, giving the partial derivative of q with respect to each component of initial position and velocity is computed, i.e.

$$S(q) = \left(\frac{\partial q}{\partial x_o}, \frac{\partial q}{\partial y_o}, \frac{\partial q}{\partial z_o}, \frac{\partial q}{\partial \dot{x}_o}, \frac{\partial q}{\partial \dot{y}_o}, \frac{\partial q}{\partial \dot{z}_o} \right). \tag{1}$$

The error sources described in Section 3 are utilized to construct covariance matrices of errors, $\wedge$. These errors are assumed uncorrelated, hence the covariance matrices, whose elements are the 3σ error estimates, are diagonal. The variance in the dependent variable is then computed as

$$\sigma^2(q) = S(q) \wedge S(q)^T. \tag{2}$$

Explicit expressions for all partial derivatives used are given in Appendix A.

4.1. Error Sensitivities

Using the partial derivative expressions derived in Appendix A, numerical partial derivatives were computed for both the IET and RET Modes at the moon and Mercury. The results are presented in Table 8. The dependent variables are listed at the head of each column with the independent variables given in the left-hand columns. The partial derivatives of periapsis radius (RP) pertain to the IET Mode. Partials

Table 8

PENETRATOR FLIGHT PARAMETER SENSITIVITIES TO DEPLOYMENT POSITION/VELOCITY

	Penetrator Flight Parameters				
	Periapse Altitude, RP(km)[a]	Braking Altitude, R(km)[b]	Impact Velocity, v(m/s)	Impact Angle, γ (deg)	Miss Distance (km)
• LUNAR CASES					
x_o(km)	2.8	1.1	11	$\sim 10^{-6}$	$\sim 10^{-4}$
y_o(km)	$\sim 10^{-7}$	0	$\sim 10^{-7}$	$\sim 10^{-5}$	1.0
z_o(km)	$\sim 10^{-7}$	0	$\sim 10^{-7}$	$\sim 10^{-5}$	1.0
$\dot{x}_o$(m/sec)	$\sim 10^{-6}$	0.4	6.7×10^{-3}	$\sim 10^{-6}$	$\sim 10^{-4}$
$\dot{y}_o$(m/sec)	4.2	$\sim 10^{-7}$	6.7×10^{-3}	0.4	0.1
$\dot{z}_o$(m/sec)	$\sim 10^{-6}$	$\sim 10^{-7}$	6.7×10^{-3}	0.4	0.1
• MERCURY CASES					
x_o(km)	0.2	7.6	25	$\sim 10^{-6}$	$\sim 10^{-10}$
y_o(km)	$\sim 10^{-8}$	0	0.01	$\sim 10^{-6}$	1.0
z_o(km)	$\sim 10^{-8}$	0	0.01	$\sim 10^{-6}$	1.0
$\dot{x}_o$(m/sec)	$\sim 10^{-6}$	137.3	6.7×10^{-3}	$\sim 10^{-6}$	$\sim 10^{-8}$
$\dot{y}_o$(m/sec)	14.6	$\sim 10^{-6}$	6.7×10^{-3}	0.4	0.04
$\dot{z}_o$(m/sec)	$\sim 10^{-8}$	$\sim 10^{-6}$	6.7×10^{-3}	0.4	0.04

a. For the IET deployment mode

b. For the RET deployment mode

of radius magnitude (R) pertain to the RET Mode. Both of these sets of partials are taken at the rest altitudes which result in a nominal impact velocity of 150 m/sec. The remaining sets of partials, for impact variables, pertain to both deployment modes.

A number of important points are observed from the data in Table 8. These can be summarized as follows:

a) The periapsis error for the IET Mode is the result of two initial errors at the ΔVA maneuver, 1) the error in the radius magnitude, x_o, and 2) the error in tangetial speed, $\dot{y}_o$;

b) With the RET Mode the error in the radius (and altitude) of the ΔVB maneuver is dominated by initial errors in, 1) the apoapsis radius, x_o, and 2) the radial speed, $\dot{x}_o$, after the ΔVA maneuver.

c) Impact speed errors result primarily from 1) errors in all components of velocity after the ΔVB maneuver, and 2) the error in the radius, x_o, at the ΔVB point;

d) The error in the impact flight path angle, γ, of the rectilinear descent results primarily from errors in the two velocity components of the ΔVB maneuver, i.e. $\dot{y}_o$ and $\dot{z}_o$. Note that the error in impact flight path angle is equivalent to the impact angle of attack for an open loop controlled penetrator on a nominally rectilinear final descent;

e) Errors in impact location, i.e. miss distance, result from the uncertainties in both the position and velocity components normal to the local radius at the completion of the ΔVB maneuver which include x_o and $\dot{x}_o$, and y_o and $\dot{y}_o$.

Taking all of these effects together, it becomes apparent that a final rectilinear descent, which is used in both modes, translates errors in every component of the state at completion of the ΔVB burn into some significant form of error in the penetrator impact conditions.

4.2. Impact Error Magnitudes

Insight into the magnitude of the final impact errors may be gleaned by combining the dominant partial derivatives of Table 8 with the magnitudes of the initial O.D. and execution errors cited in Tables 6 and 7, respectively. An illustration of these error magnitudes is presented here for the IET Mode applied to the Mercury penetrator case. Just the largest terms are analyzed to simplify the approximation of final errors. Trends in the lunar case are completely analogous.

a) Periapsis Magnitude

The net effect of initial position errors is small. The component x_o, which has the largest partial derivative, has the smallest error component while the largest errors, in y_o and z_o, have negligible partial derivatives. By far the dominant term is due to the 0.57 m/s error in $\dot{y}_o$, arising from execution of ΔVA, coupled with $\frac{\partial RP}{\partial \dot{y}_o} = 14.6$ sec. Hence

$$\Delta RP \approx \frac{\partial RP}{\partial \dot{y}_o} \Delta \dot{y}_o = 8.3 \text{ km.}$$

It should be noted that the above is the uncertainty in the magnitude of periapse radius, whereas for penetrator deployment it is the altitude which is critical. The altitude errors depend on both periapse errors and uncertainties in topography. However, the periapse error is so large that surface relative measurements are required as discussed in Section 5.

b) Impact Speed

The impact speed error due to position errors at ΔVB is most sensitive to the altitude error, Δx, as seen from Table 8. Assuming, however, that the periapse altitude of 3 km has been approached slowly with continual DSN tracking, the error in Δx is only

$$\Delta x \simeq .00006\ R_p = 150\ \text{m},$$

which leads to an impact speed error of only about 4 m/sec. The execution errors at ΔVB are large, 61-71 m/sec as seen in Table 7, but at first glance the sensitivities given in Table 8 appear to be small enough to negate any significant error contribution. Unfortunately, the linear error analysis using partial derivatives with respect to initial velocity components are valid only for small initial errors. Using the sensitivities evaluated along the nominal trajectory with the large execution errors leads to a serious underestimate of the impact speed errors.

For example, the sensitivity of impact speed, v, with respect to initial speed, v_o, can be calculated by differentiating the energy equation as

$$\frac{\partial v}{\partial v_o} = \frac{v_o}{v} .$$

Evaluating this along the nominal trajectory, i.e., $v_o = 1$ m/s and $v = 150$ m/s, gives $\frac{\partial v}{\partial v_o} = 7\text{x}10^{-3}$. Using the components in Table 7, the 3σ execution error, δv_o, at ΔVB is

$$\delta v_o = \left[70.9^2 + 61.0^2 + 70.9^2\right]^{1/2} = 117\ \text{m/sec.}$$

The linear error theory gives for the impact speed error, $\delta v = 0.8$ m/s.

However, by applying the energy equation directly, the correct impact velocity is 190 m/s for a 117 m/sec error in initial speed, which amounts to a 40 m/sec impact speed error. To illustrate the non-linearity of this sensitivity, 1σ execution errors lead to an impact speed error of only 5 m/sec.

c) Impact Flight Path Angle

This parameter is sensitive essentially only to the initial errors in $\dot{y}_o$ and $\dot{z}_o$. The dominant error here is the 61 m/sec error in y_o due to ΔVB, resulting in

$$\Delta\gamma \approx \left(\frac{\partial\gamma}{\partial y_o}\right) \Delta\dot{y}_o = 23.4^o.$$

d) Miss Distance

The error in the y and z components of position, along with the $\dot{y}$ error introduced by ΔVB, are the most significant, but the position errors, having larger partials, dominate the miss distance, D_m. Hence

$$D_m \approx \sqrt{\left(\frac{\partial(D)}{\partial y_o} \cdot \Delta y_o\right)^2 + \left(\frac{\partial(D)}{\partial z_o} \cdot \Delta z_o\right)^2} = 20.5 \text{ km},$$

where D is distance on the impact surface.

The effects of all errors on the various parameters of penetrator deployment and impact are given in Table 9 for both the IET and RET Modes for the nominal Mercury case depicted in Figure 1, page 8 . The data were calculated from equation (2) using the computer program described in Appendix B except for the impact speed errors which were calculated as described above. The results presented include the total error in each parameter along with the contribution to the total error arising from each error source considered separately.

Table 9

SUMMARY OF MERCURY PENETRATOR 3σ ERRORS DUE TO O. D./MANEUVER UNCERTAINTIES

	O. D. Error at ΔVA	Execution Error at ΔVA	O. D. Error at ΔVB	Execution Error at ΔVB	Total Deployment Error
• IET MODE					
Intermediate periapsis, RP(km)	0	8	-	-	8
Impact Speed, v(m/sec)	-	-	4	40	41
Impact path angle, γ (deg)[a]	-	-	0	36	36
Miss distance (km)	-	-	21	4	21
• RET MODE					
Braking altitude, R(km)	328	14	-	-	329
Impact speed, v(m/sec)	1320	171	-	40	1330
Impact path angle, γ (deg)[a]	13	33	-	38	52
Miss distance (km)	19	99	-	4	101

a. Path angle error equivalent to impact angle of attack

Considering the IET Mode first, the error in the intermediate periapse radius (and altitude) of more than 8 km is due primarily to execution errors of the periapse lowering maneuver, ΔVA. Since a deployment periapse altitude of only 3 km is desired, this error is obviously much too large for an acceptably safe maneuver strategy. A combination of impulsive maneuvers, perhaps including solar perturbations, to reduce the periapse altitude, with an onboard spacecraft altimeter monitoring the periapse reduction, are probably required for this deployment mode. Assuming this to be the case, the remaining three errors at impact, i.e. Δv, $\Delta\gamma$, and miss distance, result from O.D. errors at the ΔVB point and ΔVB execution errors. The only error of these three which is obviously unacceptable is the error in flight path angle, $\Delta\gamma$, of 36^{o}. Since, for open-loop control, the penetrator would be aligned after ΔVB to an attitude determined before ΔVB assuming a perfect maneuver, $\Delta\gamma$ would be equivalent to the actual angle of attack at impact. The maximum acceptable angle of attack in very soft material is about 11^{o} (see Table 1, page 2). Hence, a successful impact would occur much less than even the 1σ probability since there is an additional uncertainty in the hardness of the impact soil.

The second half of Table 9 contains summary error data for the RET Mode. It is immediately apparent that all the total errors in this mode are larger than for the IET Mode. This is primarily due to the fact that the penetrator is deployed much further from the planet (at apoapsis) allowing errors to propagate from more sources and for a longer period of time. Both the errors in impact speed and flight path angle are unacceptably high. As a point of observation, the RET Mode is generally worse than the IET Mode from an open-loop control point of view. Finally, it should be noted that the miss distance from the targeted impact point is relatively small for both deployment modes. This small error is an inherent characteristic of rectilinear trajectories.

4.3. Detailed Open-Loop Error Analysis

In an attempt to reduce the magnitude of penetrator deployment errors and to ascertain the sensitivity of these results to the various deployment input parameters, a number of off-nominal deployment cases were run for both the IET and RET Modes. Table 10a describes the conditions of each case and Table 10b and 10c give the resulting errors for lunar and Mercury missions, respectively. Two entries are given for each item within each case which pertain to the IET and RET Modes, respectively. For the IET Mode the deployment strategy includes the spacecraft lowering periapse to the desired altitude through a combination of impulsive maneuvers and solar perturbations and then releasing the penetrator. The errors are then computed based on tracking errors at the ΔVB point along with ΔVB execution errors. The comparable approach is not available for the RET Mode, since the spacecraft cannot deliver the penetrator to the ΔVB point, nor is it feasible to consider tracking, orbit determination, and a trajectory trim maneuver system for the penetrator after it has been released. Hence, errors in this mode are determined by propagating O. D. and execution errors at ΔVA to the ΔVB point and then adding ΔVB execution errors. The O. D. and execution error matrices at ΔVA have been propagated using the state transition matrix (see Appendix A).

The Mercury cases (Table 10c) are discussed first. Moving ΔVA off apoapsis makes the final errors in periapse conditions significantly worse. Changing the size of the initial orbit results in a slight improvement in the IET Mode, and significantly reduces the terminal errors in the RET Mode, although not to an acceptably small level. Reducing the magnitude of the error sources by a factor of 3 shows final errors also reduced by a similar factor. Error levels of this reduced magnitude, i. e. 0.5% (3σ) in ΔV magnitude and 0.33^{o} pointing accuracy, would be difficult to achieve in practice. Nevertheless the error levels, except for RP and

Table 10a

DETAILED ERROR ANALYSIS SUMMARY - CASE DESCRIPTIONS

Case Labels[a]	Explanations
L-1/2, M-1/2	Nominal deployment conditions; Initial orbits from Table 3, error magnitudes from Section 3, impact speed = 150 m/sec, impact flight path angle = -90^{o}, ΔVA at apoapsis of initial orbit, ΔVB at RP or R (altitudes given in Table 2).
L-3/4, M-3/4	Sensitivities to location of ΔVA point; True anomaly of ΔVA reset to 170^{o} from periapsis.
M-5/6	Sensitivities to size of initial orbit; Initial apoapsis altitude reduced from 24, 880 km to 12, 140 km corresponding to a 12-hour period about Mercury.
L-7/8, M-7/8	Sensitivities to magnitude of error sources; O. D. and execution errors reduced by a factor of 3.
L-9/10, M-9/10	Sensitivities to nominal impact flight path angle; set terminal flight path angle to -80^{o}.
L-11/12, M-11/12	Sensitivities to impact speed; increase nominal impact speed to 300 m/sec.

a. Lunar cases are identified with "L", Mercury with "M"; two subcases are run within each case class, the first (odd number) for the IET Mode, and the second (even number) for the RET Mode.

Table 10b

LUNAR ERROR RESULTS OF DETAILED ERROR ANALYSIS

Cases and Parameters	O.D. Errors at ΔVA	ΔVA Execution Errors	O.D. Errors at ΔVB	ΔVB Execution Error	Total Parameter Error
L-1/2					
R_p/R(km)	0/12	1/4	--	--	1/12
v(m/sec)	-/12	-/5	1/-	8/1	8/13
γ(deg)	-/2	-/14	0/-	15/5	15/15
Miss Distance, D_m(km)	-/14	-/18	15/-	4/1	15/23
L-3/4					
R_p/R(km)	11/5	15/3	--	--	16/6
v(m/sec)	-/12	-/7	20/-	8/8	22/16
γ(deg)	-/2	-/13	1/-	15/5	15/14
D_m(km)	-/14	-/17	14/-	4/-	15/22
L-7/8					
R_p/R(km)	0/1	0/4	--	--	1/4
v(m/sec)	-/4	-/0	0/-	1/3	1/5
γ(deg)	-/1	-/5	0/-	5/2	5/5
D_m(km)	-/5	-/6	5/-	1/0	5/8
L-9/10					
R_p/R(km)	0/4	1/0	--	--	1/4
v(m/sec)	-/11	-/5	1/-	8/1	8/12
γ(deg)	-/1	-/13	1/-	15/6	15/14
D_m(km)	-/14	-/18	15/-	4/1	15/23
L-11/12					
R_p/R(km)	0/0	1/0	--	--	1/0
v(m/sec)	-/11	-/5	1/-	4/1	4/12
γ(deg)	-/1	-/7	0/-	8/2	8/7
D_m(km)	-/14	-/7	15/-	7/2	16/16

Table 10c

MERCURY ERROR RESULTS OF DETAILED ERROR ANALYSIS

Cases and Parameters	O.D. Errors at ΔVA	ΔVA Execution Errors	O.D. Errors at ΔVB	ΔVB Execution Error	Total Parameter Error
M-1/2					
R_p/R(km)	0/328	8/14	--	--	8/329
v(m/sec)	-/1320	-/171	4/-	40/40	41/1330
γ(deg)	-/13	-/33	0/-	36/38	36/52
Miss Distance, D_m(km)	-/19	-/99	21/-	4/4	21/101
M-3/4					
R_p/R(km)	33/434	2/646	--	--	33/778
v(m/sec)	-/456	-/680	57/-	40/59	70/821
γ(deg)	-/15	-/30	2/-	36/36	36/51
D_m(km)	-/28	-/92	20/-	4/1	21/97
M-5/6					
R_p/R(km)	0/130	8/6	--	--	8/130
v(m/sec)	-/144	-/6	4/-	37/57	37/155
γ(deg)	-/12	-/22	0/-	34/36	34/44
D_m(km)	-/19	-/97	21/-	4/4	21/99
M-7/8					
R_p/R(km)	0/110	3/2	--	--	3/110
v(m/sec)	-/115	-/2	1/-	5/20	5/117
γ(deg)	-/4	-/11	0/-	12/13	12/17
D_m(km)	-/6	-/33	7/-	1/1	7/34
M-9/10					
R_p/R(km)	0/329	8/15	--	--	8/329
v(m/sec)	-/338	-/20	4/-	40/13	40/339
γ(deg)	-/14	-/30	2/-	35/36	35/50
D_m(km)	-/20	-/100	21/-	4/4	21/102
M-11/12					
R_p/R(km)	0/328	8/14	--	--	8/328
v(m/sec)	-/386	-/17	4/-	20/61	20/391
γ(deg)	-/7	-/16	0/-	18/19	18/26
D_m(km)	-/18	-/96	21/-	7/8	22/98

R, are quite acceptable for impact speed and miss distance and marginally acceptable for flight path angle. Changing the nominal impact γ to -80^{o}, i.e. the final trajectory segment no longer being vertical, results in little change in final errors, except that the error in γ is increased for the RET Mode. Increasing the nominal impact speed to 300 m/sec reduces the final γ errors by approximately a factor of two. This is intuitively reasonable since the flight path angle error is primarily determined by the tangential velocity residual after ΔVB. This residual is about the same for both the 150 m/sec and 300 m/sec impact speed cases, but the larger radial component of velocity at impact with nearly the same tangential component reduces the flight path angle error. For the higher impact speed, the final γ errors are close to allowable impact angles of attack, particularly for softer surface materials. One cautionary note needs to be injected at this point. The reduction of impact angle of attack errors by a doubling of the impact speed may be questioned, but available empirical data indicate that the limiting angle of attack can be expressed as a ratio of tangential to radial speed at impact. However, no data exists at impact speeds of 300 m/sec to indicate whether the ratio valid at 150 m/sec is also valid at 300 m/sec. Indeed it may be the case that the maximum angle of attack may decrease with increasing impact speed in which case the higher speed will not alleviate the problem.

For the lunar cases (Table 10b), similar changes in initial conditions produce comparable changes in the results. However, the initial low altitude circular orbit makes the basic situation much more favorable for open-loop penetrator deployment at the moon. The nominal cases, L-1/2, result in final errors in all parameters that are acceptable or nearly so. Of the input changes made, going to the higher impact speed, case L-11/12, resulted in a quite favorable set of final errors.

4.4. Open-Loop Deployment Summary

Open-loop deployment control of lunar penetrators produces impact errors which are very nearly within the constraints (Table 1). If impact soil properties are known to be fairly soft (S numbers > 10) and/or somewhat higher impact speeds are acceptable an open-loop control system would work. Conversely, open-loop deployment at Mercury is marginal, at best. Even if an impact speed of 300 m/sec is allowed, the IET Mode still has impact flight path angle uncertainties greater than 11^{o} (the limiting impact angle of attack cited in Table 1, page 2 . The RET Mode is not feasible, due both to large impact speed errors as well as flight path angle uncertainties. Consequently, successful open-loop penetrator deployment is unlikely via either deployment mode at Mercury. The penetrator misalignment, between the velocity vector and penetrator longitudinal axis, is dominated by uncertainties in prediction of the final velocity direction. These errors could be slashed with onboard measurements to refine the prediction of the direction of the velocity vector at impact and an active attitude control system to realign the penetrator axis with the new predicted direction. The next section discusses the type of measurements and closed-loop control needed.

5. ONBOARD PENETRATOR MEASUREMENTS FOR CLOSED-LOOP CONTROL

The previous section on open-loop error analysis pointed to the need of onboard instrumentation to reduce the errors in penetrator deployment, particularly for Mercury missions. Two types of measurements are needed: 1) altimeter measurements to determine topographic relative altitudes for penetrator deployment at the ΔVB point, and 2) residual velocity measurements after the ΔVB maneuver to ascertain the direction of the impact velocity vector in order to reduce impact angle of attack errors.

A radar altimeter is an obvious choice for altimetry measurements. It would be required to have a maximum range of only a few tens of kilometers and a minimum range of about 1 km. Range measurement accuracies to the order of 1% are sufficient. Small weight and power requirements are essential. A radar altimeter design that is quite acceptable in meeting these constraints is described in reference 5. A summary of the pertinent characteristics of this instrument is given in Table 11. The instrument was developed under NASA contract primarily for use in altimeter measurements in meteorological balloons and as such is not yet space qualified hardware. It could be used to give surface relative altitude in either the IET or RET Modes for determining the altitude for performing ΔVB. If the penetrator is released at apoapsis and falls to the ΔVB point as defined by the RET Mode, the altimeter would necessarily be part of the penetrator deployment system. However, if the spacecraft delivers the penetrator to the ΔVB point as defined by the IET Mode, the altimeter would be part of the spacecraft and could be used for multiple penetrator deployments.

Table 11

RADAR ALTIMETER CHARACTERISTICS[a]

Mass (including antenna)	160 g
Maximum Range	>18 km
Absolute Accuracy	± 10 m
Power Required	0.7 w
RF Frequency	415 MHz
Operating Temperature Range	-55° to 55°C

a. Reference 5

Table 12

PENETRATOR IMPACT ERRORS WITH RADAR ALTIMETRY

Case and Parameters	O.D. Error at ΔVA	ΔVA Execution Error	O.D. Error at ΔVB	ΔVB Execution Error	Error
L-1/2					
v(m/sec)	--	-/5	1/-	8/1	8/6
γ (deg)	-/2	-/14	0/-	15/5	15/15
D_m (km)	-/14	-/18	15/-	4/1	15/23
M-1/2					
v(m/sec)	--	-/32	4/-	41/41	41/66
γ (deg)	-/13	-/32	0/-	23/38	36/52
D_m (km)	-/19	-/99	21/-	4/4	21/101

Table 12 gives the effect of including altitude measurements on the terminal errors. The altitude measurements were simulated by reducing σ of the ΔVB altitude to 0.03 km in the O.D. error matrix and in the error covariance resulting from propagation of ΔVA errors to the ΔVB point. Correlations between position and velocity must also be considered. For example, measurement of altitude means that the position of the penetrator is determined to an accuracy limited primarily by uncertainties in planetary topography. Knowing the altitude of the penetrators permits determination of its speed to an accuracy consistent with initial error sources. For Mercury, the speed prior to ΔVB is insensitive to the assumed O.D. error sources and to errors in Mercury's topography on the order of 1 km. However, execution of ΔVA introduces a tangential velocity error which propagates to nearly 103 m/sec at the ΔVB point. This error, together with ΔVB execution errors, is now the dominant source of impact errors. It can be seen in Table 12 that the addition of altitude measurements results in a substantial reduction in impact speed errors but has little effect on other errors. This is because impact speed errors, particularly in the RET Mode, result from errors in the altitude of the ΔVB point which are significantly reduced by making altitude measurements. Errors in flight path angle, γ, and miss distance, D_m, are dominated by errors in the horizontal velocity. These errors are essentially unaffected by altitude measurements.

Determination of the flight path angle, γ, at impact requires knowledge of the relative horizontal ground speed, v_t, of the penetrator after ΔVB has been performed. If v_t is measured immediately after ΔVB, which occurs at an altitude H, then γ at impact is determined from:

$$\tan \gamma = \frac{v_{rs}}{(1 + \frac{H}{R_s})v_t}, \qquad (3)$$

where v_{rs} is the radial velocity component and R_s is the surface radius of the planet. Using the nominal value of v_{rs} in equation (3), then allows γ to be predicted. The horizontal speed may be measured in one of two ways: 1) onboard measurement of the maneuver execution velocity errors, or 2) direct measurements of the horizontal speed relative to the surface.

5.1. Closed-Loop Attitude Control with Accelerometers

The first method is possible since the largest contribution to the residual horizontal velocity arises from execution errors in performing ΔVB, hence measurement of the velocity residuals gives a good estimate of v_t. These errors could be measured through the use of onboard accelerometers. To ascertain measurement accuracies of onboard accelerometers for penetrator deployment the representative error characteristics given in Table 13 were used.

Calculation of velocity measurement accuracies also requires knowledge of the accelerations involved in performing the maneuvers. Several solid propulsion systems having mass of the order required for ΔVB at Mercury have been developed for space applications. Thrust levels on representative systems vary from about 17,000 newtons to 170,000 newtons, with burn times from around 3-20 seconds and would give peak accelerations of 33-330 g's. Table 14 gives the resulting errors in velocity measurements of ΔVB of the IET Mode at Mercury for the high thrust level (170,000 newtons) based on the error sources of Table 13. The smaller thrust level would result in increasing the bias error to 3×10^{-2} m/sec, which is still negligibly small. Although various types of accelerometers have different error characteristics, the above analysis

Table 13

TYPICAL ACCELEROMETER ERROR CHARACTERISTICS

Bias	1×10^{-4} g's
Scale Factor	5×10^{-5} g's/g
Misalignment	80 arc sec

Table 14

ACCELEROMETER MEASUREMENT ERRORS OF ΔVB[a]

	Bias	Scale Factor	Misalignment
$\Delta \dot{x}$(m/sec)	0	0	1.6
$\Delta \dot{y}$(m/sec)	3×10^{-3}	0.2	0
$\Delta \dot{z}$(m/sec)	0	0	1.6

a. Mercury IET Mode; nominal ΔVB = 4065 m/sec

Table 15

IMPACT ANGLES OF ATTACK USING ACCELEROMETERS[a]

Case and Parameter	O.D. Error at ΔVA	ΔVA Execution Error	O.D. Error at ΔVB	ΔVB Execution Error	Total Error
M1					
α(deg)[b]	-	-	0.09	1.12	1.12
L1					
α(deg)	-	-	0	1.10	1.10

a. IET Mode only

b. $\alpha \equiv$ impact angle of attack

indicates that the velocity measurement errors will be at most 2-3 m/sec per axis. Measurements of this accuracy are quite sufficient to reduce the effects of maneuver execution errors on the impact angle of attack to acceptable levels.

In Section 4 it was noted that there are two components to the residual tangential speed: 1) an in-plane component in the direction of the ΔVB vector arising from impulse errors in the burn magnitude, and 2) an out-of-plane component due to thrust misalignment. These residuals are of nearly equal magnitude and both would have to be measured. This requires two accelerometers and probably a three accelerometer system would be simplest to mechanize with gyros. A strapdown system with the accelerometers and gyros attached directly to the penetrator frame would be well suited as this system offers weight saving at the expense of some measurement accuracy.

Table 15 summarizes the impact angle of attack errors for the IET Mode based on accelerometer measurements of all three velocity components and the measurement accuracies described above. Following the ΔVB burn, the penetrator reorients to the path angle and azimuth determined by measuring velocity components. Assuming 3σ final attitude control pointing errors of 1^{o}, the 3σ angle of attack error at either the moon or Mercury would be less than 2^{o}. This error is well within the 3^{o} constraint for impacts in very hard soils, e.g. basaltic lava. Note, however, that the impact flight path angle errors presented in Table 12 are unchanged by either the radar altimeter or accelerometer measurements. While penetration can probably be achieved, the resulting penetrator angle at rest may be unacceptable for some experiments, particularly at Mercury where the 3σ γ errors are considerably larger than the desired 15^{o} limit cited in Table 1, page 2 .

5.2. Closed-Loop Attitude Control with Driftmeters

The second method of measuring the residual horizontal velocity after ΔVB is a passive optical technique employed by driftmeters (v_t/H meters). Specifically, optical driftmeters measure the ratio v_t/H, where v_t is the horizontal velocity at the altitude H. These devices have also been considered for determination of attitude rates of orbiting spacecraft[7]. The basic technique consists of an optical system to form the image of the surface onto a reticle consisting of alternate opaque and transparent bands and then onto a photodetector. Motion of the v_t/H meter parallel to the surface moves the image across the banded surface, which effectively chops the image to produce an output signal whose average frequency is proportional to v_t/H. Measurements of v_t/H can then be combined with radar altimeter measurements of H to determine v_t and consequently allow prediction of γ.

The measurement accuracy required in order to meet the most stringent angle of attack constraint of 3^o may be estimated by differentiating equation (3) above, yielding

$$\sec^2\gamma\,\delta\gamma = \frac{\delta v_{rs}}{(1+\frac{H}{R_s})v_t} - \frac{v_{rs}\,\delta v_t}{(1+\frac{H}{R_s})v_t^2}$$

$$- \frac{v_{rs}}{(1+\frac{H}{R_s})^2 v_t}\,\frac{\delta H}{R_s} \qquad (4)$$

For Mercury, $H/R_s = .0012$ and $\frac{\delta H}{R_s} \approx 5\times10^{-5}$, assuming for δH, a conservative estimate of the 3σ altimeter error of 0.1 km. Neglecting these terms, equation (4) simplifies to

$$\sec^2\gamma\delta\gamma \approx \frac{\delta v_{rs}}{v_t} - \frac{v_{rs}}{v_t}\frac{\delta v_t}{v_t} \tag{5}$$

For these terms to be approximately equal in magnitude requires that $\frac{\delta v_t}{v_t} \sim \frac{\delta v_{rs}}{v_{rs}}$. Using a value of 150 m/sec for v_{rs} and an uncertainty of 18 m/sec for δv_{rs} results in $\frac{\delta v_t}{v_t} \sim 0.12$. These values come from the nominal Mercury IET Mode where the 18 m/sec error in radial impact speed results from a 3σ residual radial velocity of 71 m/sec after ΔVB (see Table 7, page 20). The uncertainty in the δv_t measurement arises from errors in measurement of v_t/H, and $\delta(v_t/H)$, together with altitude measurement uncertainties δH. Since

$$\frac{\delta v_t}{v_t} = \frac{\delta(v_t/H)}{v_t/H} + \frac{\delta H}{H}, \tag{6}$$

and our estimate of $\delta H/H$ is 0.03 at Mercury, then for a value of 0.12 for $\delta v_t/v_t$ equation (6) provides

$$\frac{\delta(v_t/H)}{v_t/H} = 0.09.$$

Hence, a driftmeter measurement accuracy of about 10% is sufficient to reduce the uncertainties in the predicted value of γ to the same level as those resulting from the unmeasured radial speed residual after ΔVB.

The above discussion is valid only if the residual tangential speed after ΔVB is aligned with the penetrator mounted driftmeter. In general, errors introduced by the ΔVB burn will also contain an out-of-plane component in the tangential velocity, v_t, perpendicular to this direction.

Therefore, two orthogonal driftmeters are required to sense the true magnitude of v_t. The impact attitude (angle of attack) errors resulting from closed-loop attitude control using a pair of driftmeters are summarized in Table 16 for the IET Mode at the moon and Mercury for three levels of driftmeter accuracy: 5, 10, and 15%. Note that these results are based on a nominal impact velocity of 150 m/sec, a 3σ error in the radial impact speed, and an inherent 1^{o} error in the attitude control system pointing accuracy. Results are given for three levels of residual tangential velocity. From Table 7, page 20, 3σ residual tangential velocities at the moon and Mercury are expected to be 39 m/sec and 94 m/sec, respectively. Comparing these values with the data in Table 16, driftmeter supported closed-loop attitude control can be expected to reduce impact angle of attack errors to 4^{o} at the moon and 9^{o} at Mercury. Recalling that closed-loop attitude control with an accelerometer triad reduces angle of attack errors to about 2^{o} at either target, it can be seen that accelerometers are preferred to driftmeters, particularly if harder impact soils are expected where the maximum angle of attack error should be less than 3^{o}. This conclusion is strengthened by the fact that accelerometers are completely independent of target surface features (shadowing) and provide results which are less sensitive to the radar altitude measurement. Note that the angle of attack errors using accelerometers is nearly the same as the systematic error introduced in Section 2 by ignoring the rotational velocity of the primary. However, targeting the final trajectory segment to allow for the finite rotational speed would eliminate the systematic error but there would still remain the random angle of attack errors.

Table 16

IMPACT ANGLES OF ATTACK USING DRIFTMETERS[a]

Target	$\frac{\delta(v_t/H)}{v_t/H}$	v_t	$2v_t$	$3\ v_t$
• Moon (IET Mode, v_t = 13 m/sec)				
	0.05	1.2^o	1.7^o	2.3^o
	0.10	1.6^o	2.6^o	3.7^o
	0.15	2.1^o	3.7^o	5.3^o
• Mercury (IET Mode, v_t = 30 m/sec)				
	0.05	3.0^o	5.3^o	6.8^o
	0.10	3.8^o	6.9^o	8.9^o
	0.15	4.8^o	8.8^o	11.5^o

a. Results include a 1^o attitude control pointing error

6. SUMMARY AND CONCLUSIONS

The error analysis of penetrator deployment from orbiting spacecraft at targets without atmospheres yields a number of significant results. First, the Intermediate Ellipse Transfer (IET) Mode is preferable both from the viewpoint of minimum ΔV requirements and deployment errors. Second, open-loop error analysis indicates that when the penetrator is deployed at apoapsis and coasts on its own to the ΔVB maneuver point, large errors occur in the impact speed and flight path angle. At Mercury the errors are unacceptably large, whereas for lunar deployment the flight path angle errors are marginally acceptable for impacts into soft material, but are too large for impacts into rocky surfaces. The terminal errors in impact speed are significantly reduced if the spacecraft can deliver the penetrator to the second maneuver point, thereby eliminating the effects of initial O. D. errors and maneuver execution errors at ΔVA. For Mercury orbiters it may be possible to utilize solar perturbations on the orbit to smoothly reduce periapse at small rates in order to attain the low 3 km periapse altitude required for penetrator deployment. While this deployment mode is preferred from the viewpoint of reducing penetrator errors, the effect of orbit orientation constraints on the overall mission design must be examined. The largest open-loop error is in the angle of attack at impact. This error arises primarily from errors in the predicted flight path angle at impact due to the horizontal velocity errors introduced by the ΔVB maneuver. These errors are due to out-of-plane pointing errors in performing ΔVB and to errors in the magnitude of the ΔVB impulse. A second problem area for Mercury deployment is the magnitude of the flight path angle at impact. This angle should be no greater than 15° from the vertical, whereas the 3σ errors are 36°. This can only be controlled, in the absence of propulsive maneuvers, by using a higher impact speed or by reducing the impulse variations of

the rocket engine and out-of-plane pointing errors. Finally, the errors in impact speed are near the limits of acceptability. These errors can be reduced only by reducing the error sources in ΔVB just noted, again assuming no corrective propulsive maneuvers.

Orbiter altitude measurements are required for precise determination of the ΔVB maneuver altitude. For both lunar and Mercury penetrator deployment an onboard determination of the impact flight path angle is required in order to reduce penetrator angle of impact attack errors. Onboard accelerometers measuring the velocity residuals after ΔVB provide an accurate measurement of the primary error source for the impact angle of attack. An alternative onboard measurement technique using optical driftmeters, in conjunction with altimeter measurements, cannot reduce the angle of attack errors to acceptable levels for all cases.

Although higher impact speeds are desirable from the viewpoint of reducing errors in the impact flight path angle and allowing higher rest altitudes, they quickly lead to difficulties with the penetrator design. As discussed in Section 2, doubling the impact speed from the nominal value of 150 m/sec to 300 m/sec would exceed the deceleration limit of 2000 g's in rocky soil and the penetration depth of 15-20 m in soft soils. Changing the penetrator diameter would solve the problem at one end but make it worse at the other end. Also, the penetrator forebody diameter of the Mars design is only 9 cm, so making it any smaller to ease g-loads in hard soils would also create new payload packaging problems.

One final area of concern was identified but not analyzed. It involves the response time of the attitude control system. Immediately after the ΔVB maneuver the onboard control system of the penetrator must reduce the accelerometer measurements to the desired penetrator orientation, nominally about 90^{o} from the horizontal ΔVB maneuver attitude. Then the attitude control system must pitch the penetrator to

this attitude, damp out over/under-shoot errors and do so with enough time to jettison all systems external to the penetrator itself (31 kg) before impact. This jettison must occur sufficiently early and with enough speed to guarantee that impacts of the excess parts do not interfere with the penetrator afterbody or its antenna, either by hitting it directly or through ejecta created by their impacts. The nominal fall times for a 150 m/sec impact speed, are 41 sec at Mercury and 93 seconds at the moon. Using the 3σ estimates of the error in the radial component of velocity from Tables 6 and 7, (page 20), and assuming that the error is directed toward the surface, the fall times drop to 26 seconds at Mercury and 76 seconds at the moon. Whether or not this is sufficient time to accomplish all the operations just described successfully is a question of feasibility which has not been analyzed. To do so will require a more detailed definition of the penetrator design and its mass properties for Mercury missions.

In conclusion, the deployment of lunar penetrators appears to pose no unreasonable performance or control requirements. Conversely, the low deployment altitude, large retro mass, large retro execution errors, and short descent time, all raise fundamental feasibility questions for a Mercury penetrator mission. For either concept more detailed design and error analysis will be required before serious mission planning can reasonably be considered and is recommended.

REFERENCES

1. "Mars Penetrator: Subsurface Science Mission", Report No. SAND-74-0131, Sandia Laboratories, August, 1974.

2. Friedlander, A. L., W. K. Hartmann and J. C. Niehoff, "Pioneer Mars 1979 Mission Options", SAI Report No. 120-M1, January, 1974.

3. "Pioneer Mars Surface Penetrator Mission", Report No. D2546, Hughes Aircraft/Space and Communications Group, August, 1974.

4. Asnin, S. K. and D. G. Roos, "Mission Design and Navigation for a 1977-1978 Venus Swingby/Mercury Orbiter", J. Spacecraft and Rockets, 10, 1. 631-637, October, 1973.

5. Levanon, N., F. G. Stremler and V. E. Suomi, "A New Approach to Lightweight Radar Altimeters", Proc. IEEE, 62, p. 784-792, June, 1974.

6. Goodyear, W. H., "Completely General Closed-Form Solution for Co-ordinates and Partial Derivatives of the Two-Body Problem", Astron. J., 70, p. 189-192, April, 1965.

7. Button, P. A., P. E. Mallory, and J. B. Boor, "V/H Satellite Attitude Control", Proc. National Specialist's Meeting on Guidance of Aerospace Vehicles, IAS, Boston, pp. 114-120, 1960.

8. Escobol, P. R., Methods of Orbit Determination, Wiley and Sons, 1965.

APPENDIX A: FORMULATION OF PARTIAL DERIVATIVES

To determine the effects of the various error sources on the final variables of interest (periapse radius, radius magnitude, speed, flight path angle and miss distance), the partial derivatives of the final variables with respect to the initial position and velocity components are needed. Fundamental to the calculation of several of these derivatives is the state transition matrix, which is a 6x6 matrix of the partial derivatives of the position vector, $\bar{r}$, and velocity vector, $\bar{v}$, with respect to an initial position vector, $\bar{r}_o$, and initial velocity vector, $\bar{v}_o$, along a Keplerian trajectory. A formulation of the state transition matrix in universal variables, based upon reference 6, was utilized to compute the partial derivatives, $\frac{\partial \bar{r}}{\partial \bar{r}_o} = \left(\frac{\partial x}{\partial x_o}, \frac{\partial x}{\partial y_o}, \frac{\partial x}{\partial z_o}, \frac{\partial y}{\partial x_o}, \text{etc.}\right)$, etc. for all of the required 36 elements. These derivatives were available for use in the calculation of the partials derived below.

Periapse Partial Derivatives

The derivatives of periapse radius, RP, with respect to the initial state vector, i.e. $\frac{\partial RP}{\partial x_o}$, $\frac{\partial RP}{\partial y_o}$, $\frac{\partial RP}{\partial z_o}$, $\frac{\partial RP}{\partial \dot{x}_o}$, $\frac{\partial RP}{\partial \dot{y}_o}$, and $\frac{\partial RP}{\partial \dot{z}_o}$ were required. Using RP = a (1-e), then

$$\frac{\partial RP}{\partial x_o} = \frac{\partial a}{\partial x_o}(1-e) - a\frac{\partial e}{\partial x_o} \quad . \qquad \text{A.1}$$

From the energy relation $\frac{v^2}{2} - \frac{\mu}{r} = -\frac{\mu}{2a}$, one has A.2

$$\frac{\partial a}{\partial x_o} = \frac{2a^2 x_o}{r_o^3} \, .$$

The $\frac{\partial e}{\partial x_o}$ term may conveniently be evaluated in terms of the partial derivatives of two other functions, C_e and S_e, which are tabulated in reference 8, p. 331. Now from the definitions $C_e = e \cos E$, $S_e = e \sin E$, where E is the eccentric anomaly, we have

$$\frac{\partial C_e}{\partial x_o} = \frac{\partial e}{\partial x_o} \cos E - e \sin E \frac{\partial E}{\partial x_o} \qquad \text{A.3}$$

$$\frac{\partial S_e}{\partial x_o} = \frac{\partial e}{\partial x_o} \sin E + e \cos E \frac{\partial E}{\partial x_o} \; . \qquad \text{A.4}$$

Multiplying A.3 by cos E and A.4 by sin E and adding gives

$$\frac{\partial e}{\partial x_o} = \frac{\partial C_e}{\partial x_o} \cos E_o + \frac{\partial S_e}{\partial x_o} \sin E_o \; . \qquad \text{A.5}$$

From reference 8, $$\frac{\partial C_e}{\partial x_o} = \frac{x_o v_o^2}{\mu r_o} \; , \qquad \text{A.6}$$

$$\frac{\partial S_e}{\partial x_o} = \frac{\dot{x}_o}{\sqrt{\mu a}} - \frac{a S_e x_o}{r_o^3} \qquad \text{A.7}$$

Combining A.1, A.2, A.5, A.6 and A.7 yields

$$\frac{\partial RP}{\partial x_o} = \frac{2a^2 x_o(1-e)}{r_o^3} - a\left[\frac{x_o v_o^2}{\mu r_o}\cos E_o + \sin E_o\left(\frac{\dot{x}_o}{\sqrt{\mu a}} - \frac{a S_e x_o}{r_o^3}\right)\right] \qquad \text{A.8}$$

The partials $\frac{\partial RP}{y_o}$, $\frac{\partial RP}{z_o}$ may be found from A.8 by replacing $(x_o, \dot{x}_o)$ by $(y_o, \dot{y}_o)$ and $(z_o, \dot{z}_o)$ successively.

The velocity partials may be found in an anologous manner. The energy relation may again be employed to determine

$$\frac{\partial a}{\partial \dot{x}_o} = \frac{2a^2 \dot{x}_o}{\mu} \quad .$$

Then

$$\frac{\partial RP}{\partial \dot{x}_o} = \frac{2a^2 \dot{x}_o (1-e)}{\mu} - a\left[\frac{2r_o \dot{x}_o}{\mu}\cos E_o + \sin E_o\left(\frac{x_o}{\sqrt{\mu a}} - \frac{a S_e \dot{x}_o}{\mu}\right)\right] \qquad \text{A.9}$$

Again the remaining partials, $\frac{\partial RP}{y_o}$ and $\frac{\partial RP}{z_o}$ are found by replacing $(x_o, \dot{x}_o)$ with $(y_o, \dot{y}_o)$ and $z_o, \dot{z}_o)$.

Radius and Velocity Partial Derivatives

From the relation $R^2 = x^2 + y^2 + z^2$

$$\frac{R}{x_o} = \frac{1}{R}\left[x \frac{\partial x}{\partial x_o} + y \frac{\partial y}{\partial x_o} + z \frac{\partial x}{\partial x_o} \right] . \qquad \text{A.10}$$

As the elements $\frac{\partial x}{\partial x_o}$, etc. are available from the state transition matrix, these partial derivatives of R are straightforward. Similarly, using

$$v^2 = \dot{x}^2 + \dot{y}^2 + \dot{z}^2,$$

$$\text{then } \frac{\partial v}{\partial x_o} = \frac{1}{v}\left[\dot{x} \frac{\partial \dot{x}}{\partial x_o} + \dot{y} \frac{\partial \dot{y}}{\partial x_o} + \dot{z} \frac{\partial \dot{z}}{\partial x_o} \right] , \qquad \text{A.11}$$

and the derivatives $\frac{\dot{x}}{x_o}$, etc. are obtained from the state transition matrix. The other partial derivatives are obtained by replacing x_o by y_o, z_o, $\dot{x}_o$, $\dot{y}_o$, and $\dot{z}_o$ successively.

Flight Path Angle Partial Derivatives

From the definition of the flight path angle γ, one has

$$\sin \gamma = \frac{\bar{r} \cdot \bar{v}}{rv} .$$

Forming the partial derivative with respect to x_o,

$$\cos \gamma \frac{\partial \gamma}{\partial x_o} = \frac{1}{rv} \frac{\partial(\bar{r} \cdot \bar{v})}{\partial x_o} - \frac{\bar{r} \cdot \bar{v}}{(rv)^2} \frac{\partial(rv)}{\partial x_o} . \qquad \text{A.12}$$

Now

$$\frac{\partial(r \cdot v)}{\partial x_o} = \frac{\partial(x\dot{x} + y\dot{y} + z\dot{z})}{\partial x_o} = \dot{x}\frac{\partial x}{\partial x_o} + x\frac{\partial \dot{x}}{\partial x_o} + \dot{y}\frac{\partial y}{\partial x_o}$$

$$+ y\frac{\partial \dot{y}}{\partial x_o} + \dot{z}\frac{\partial z}{\partial x_o} + z\frac{\partial \dot{z}}{\partial x_o} \quad . \qquad \text{A. 13}$$

Equation A. 13 may be evaluated using the state transition matrix. The term $\frac{\partial(rv)}{\partial x_o}$ in Equation A. 12 can be expressed as

$$\frac{\partial(rv)}{\partial x_o} = v\frac{\partial r}{\partial x_o} + r\frac{\partial v}{\partial x_o} \quad . \qquad \text{A. 14}$$

Note that $\frac{\partial r}{\partial x_o}$ and $\frac{\partial v}{\partial x_o}$ have been previously evaluated in Equations A. 10 and A. 11. Hence, combining A. 12, A. 13 and A. 14 yields

$$\frac{\partial \gamma}{\partial x_o} = \frac{1}{rv\cos\gamma}\left(\dot{x}\frac{\partial x}{\partial x_o} + x\frac{\partial \dot{x}}{\partial x_o} + \dot{y}\frac{\partial y}{\partial x_o} + y\frac{\partial \dot{y}}{\partial x_o}\right.$$

$$\left. + \dot{z}\frac{\partial z}{\partial x_o} + z\frac{\partial \dot{z}}{\partial x_o}\right) - \frac{(x\dot{x}+y\dot{y}+z\dot{z})}{(rv)^2\cos\gamma}\left(v\frac{\partial r}{\partial x_o} + r\frac{\partial v}{\partial x_o}\right) \qquad \text{A. 15}$$

The other partials may again be found by successively replacing $(x_o, \dot{x}_o)$ in A. 15 by $(y_o, \dot{y}_o)$ and $(z_o, \dot{z}_o)$.

Miss Distance Partials

Let the polar co-ordinates of the impact point be α, δ, where $\sin\delta = z/R_{planet}$ and $\tan\alpha = y/x$ with x, y, z being planetocentric cartesian co-ordinates.

Then

$$\cos\delta \frac{\partial\delta}{\partial x_o} = \frac{1}{R_{planet}} \frac{\partial z}{\partial x_o}$$

and

$$\sec^2\alpha \frac{\partial\alpha}{\partial x_o} = \frac{\partial y/\partial x_o}{x} - \frac{y}{x^2} \frac{\partial x}{\partial x_o}$$

or,

$$\frac{\partial\alpha}{\partial x_o} = \cos^2\alpha \left(\frac{1}{x} \frac{\partial y}{\partial x_o} - \frac{y}{x^2} \frac{\partial x}{\partial x_o} \right) .$$

Now for a small change Δx_o, the change in the impact point or miss distance (D_m) is:

$$\Delta D_m = R_{planet}\, \Delta\theta = R_{planet} \left[(\Delta\delta)^2 + \cos^2\delta\, (\Delta\alpha)^2 \right]^{1/2}$$

$$= R_{planet} \left[\left(\frac{\partial\delta}{\partial x_o} \right)^2 + \cos^2\delta \left(\frac{\partial\alpha}{\partial x_o} \right)^2 \right]^{1/2} \Delta x_o .$$

Hence,

$$\frac{\partial D_m}{\partial x_o} = R_{planet} \frac{\partial\theta}{\partial x_o} = R_{planet} \left[\left(\frac{\partial\delta}{\partial x_o} \right)^2 + \cos^2\delta \left(\frac{\partial\alpha}{\partial x_o} \right)^2 \right]^{1/2} \qquad \text{A. 16}$$

The other partials are obtained as before.

Equations A. 15 and A. 16 become indeterminate (zero over zero) along rectilinear trajectories. In such cases the partial derivatives are computed numerically.

APPENDIX B: ERROR ANALYSIS COMPUTER PROGRAM

A program was developed on the CDC 6400 computer to compute the maneuver ΔV's, O.D. and execution errors, and errors in the dependent variables. The required program inputs are given in Table B-1. The program first computes the nominal ΔVA and ΔVB maneuvers, the intermediate and terminal trajectories and impact conditions based on conic trajectories. From the position and velocity at the ΔVA and ΔVB points and ΔVA and ΔVB magnitudes, O.D. and execution error covariance matrices are calculated. The errors are assumed to be uncorrelated, hence these are diagonal matrices. Next, the partial derivatives are evaluated along the trajectory after the ΔVA maneuver has been performed. The formulation of partial derivatives is given in Appendix A. Based on these partials and the O.D. and execution errors at the ΔVA point the error in the ΔVB maneuver radius is determined. The O.D. covariance and ΔVA execution covariance matrices are also propagated to the ΔVB point utilizing the state transition matrix evaluated along the intermediate trajectory. The state transition matrix is based upon a formulation in universal variables (and consequently is valid along any conic trajectory) as described in Reference 6. Finally, the program calculates the partial derivatives along the final trajectory segment and determines errors in the impact parameters.

Program output consists of conic trajectory parameters and ΔV's, error sources for O.D. and execution errors, partial derivatives along both trajectory segments and resulting errors in periapse radius, impact speed, impact flight path angle, impact angle of attack, and miss distance. Table B-2 lists the specific program outputs.

Table B-1

ERROR ANALYSIS PROGRAM INPUTS

Variable Name	Units	Description
GMU	km^3/sec^2	Gravitational parameter of the target body
RAO	km	Apoapse radius of initial orbit
RPO	km	Periapse radius of initial orbit
RPLAN	km	Radius of target body
MODE	-	= 1 for I.E. Mode = 2 for R.E. Mode
VINOM	km/sec	Nominal impact speed
GAMINOM	deg	Nominal impact flight path angle
RPINT	km	Periapse radius of intermediate ellipse for I.E. mode
RINT	km	Radius of ΔVB maneuver point
TAO	deg	True anomaly of ΔVA maneuver point in initial orbit
EXERR(2)	-	Fractional error in magnitude of ΔVA and ΔVB
OOPPE(2)	deg	Out of plane pointing error for ΔVA and ΔVB maneuvers.
IPEE(2)	deg	Inplane pointing error for ΔVA and ΔVB maneuvers

Table B-1 (Concluded)

ERROR ANALYSIS PROGRAM INPUTS

Variable Name	Units	Description
ODCVCHG	-	Numerical multiplier used for changing magnitude of O.D. errors
SIGATT	deg	3σ error in attitude control system pointing errors
IENDFL	-	Set to 1 on last case to terminate run

Table B-2

ERROR ANALYSIS PROGRAM OUTPUTS

A. Nominal Conditions

Initial position and velocity vectors

ΔVA and ΔVB vectors

Position and velocity vector at ΔVB

Velocity vector after ΔVA and ΔVB

Semimajor axis, eccentricities and flight times along both trajectory segments

B. Error Sources

Orbit determination error matrix at ΔVA point, ΔVB point and ΔVA errors propagated to ΔVB

Execution error matrix for ΔVA and ΔVB maneuvers and ΔVA errors propated to ΔVB

C. Dependent Variable Sensitivities

Partial derivatives of R, RP with respect to initial position and velocity vector components computed along the trajectory from ΔVA to ΔVB

Partial derivatives of impact speed, flight path angle and miss distance with respect to position and velocity vector components along the trajectory from ΔVA to impact

D. Error Independent Variables

Total error and errors due to individual sources are computed for:

- o ΔVB maneuver altitude
- o Impact speed
- o Impact flight path angle
- o Impact angle of attack
- o Miss distance